Novel Quaternary Metal-Rich Phosphides: Stabilization by Differential Fractional Site Occupancies and Polar Intermetallic Bonding

Holger Kleinke[†] and Hugo F. Franzen*

Contribution from the Ames Laboratory, DOE−Iowa State University, Ames, Iowa 50011

Received June 6, 1997[⊗]

Abstract: The new phosphide $Hf_5Nb_5Ni_3P_5$ has been prepared by arc-melting of a pressed stoichiometric mixture of HfP, Nb, and Ni. Single crystals suitable for the structure determination were obtained after annealing in an induction furnace at 1350 °C. $Hf_5Nb_5Ni_3P_5$ crystallizes in the hexagonal space group $P\bar{6}2m$ (No. 189). The early transition metal atoms Hf and Nb are found on three crystallographically different sites, with refined occupancies of 100% Hf for the M1, 59.5(4)% Hf and 40.5(4)% Nb for the M2, and 13.1(6)% Hf and 86.9(6)% Nb for the M3 site. Small variations of the Hf to Nb ratio are possible, occurring with significantly different lattice parameters. The early transition elements form a three-dimensional framework with numerous M−M (M = Hf, Nb) interactions, including Ni and P in its trigonal prismatic voids. The differential fractional site occupancies can be understood on the basis of the different preferences of Hf and Nb to form M−M, M−Ni, and M−P bonds. The metallic character is confirmed by the Pauli paramagnetism experimentally obtained.

Introduction

The model of differential fractional site occupancies (DFSO) was first used to explain the occurrence of new structure types in the quasibinary system Nb−Ta−S which are unknown among the binary sulfides. The four sulfides $Nb_{1.72}Ta_{3.28}S_2$,[1] $Nb_{0.95}Ta_{1.05}S_2$,[2] $Nb_{4.92}Ta_{6.08}S_4$,[3] and $Nb_{6.74}Ta_{5.26}S_4$[4] all have no counterpart among the binaries, although Nb and Ta are closely related metal atoms. The three criteria for DFSO stabilized materials are as follows: (i) each metal atom site is statistically occupied by two different metal atoms, (ii) the fractional site occupancies per site are more or less fixed, but differ from one site to another, and (iii) the structures of the DFSO materials are unknown in the binary systems.

The similarity of Nb and Ta enables mixed Nb/Ta occupancies on each metal site in these sulfides, but the metals are apparently different enough to show clear preferences for the different metal sites. It has been shown by calculating the Pauling bond orders (PBO) and the Mulliken overlap populations (MOP), using the extended Hückel approximation, that the Nb/Ta ratio increases with decreasing metal−metal interactions.[5,6] The preference of Ta for the sites with more metal−metal interactions is based on the greater extension of its 5d orbitals, compared to the Nb 4d orbitals.

The DFSO concept is not limited to sulfides of metal pairs of the same group. Recently, two new structure types have been uncovered with $Zr_{6.45}Nb_{4.55}P_4$[7] and $Hf_{5.08}Mo_{0.92}P_3$.[8] In both cases, the more electron rich metal atom (Nb and Mo, respectively) prefers the sites with higher metal−metal bond order. On the other hand, the isostructural ZrNbP and HfNbP (Co_2Si type) show complete ordering on the metal sites.[9] To date, the DFSO concept has only been applied in quasibinary systems. Expanding the DFSO concept to quasiternary systems seemed to us to be promising, because several ternary pnictides and chalcogenides with new structure types and interesting physical and structural properties have been uncovered in the past. The ternaries, consisting of an early and a late transition metal atom and a nonmetal atom, are stabilized by strong early−late transition metal bonds, which correspond to Lewis' acid/base concept. The structures of $Nb_9Ni_{2-x}S_{3+x}$,[10] $Ta_9M'_2S_6$ (M′ = Fe, Co, Ni),[11,12] $Ta_{11}M'_2Se_8$ (M′ = Fe, Co, Ni),[13] Ta_8NiSe_8,[14] $Zr_6M'Te_2$ (M′ = Mn, Fe, Co, Ni, Ru, Pt),[15] $Hf_8M'Te_6$ (M′ = Mn, Fe),[16] $Hf_5M'Te_3$ (M′ = Fe, Co),[17] $M_2M'P$,[18,19] $Hf_5Co_{1+x}P_{3-x}$,[20] $Hf_5Ni_{1+x}P_3$,[21] $Zr_9M'_2P_4$ (M′ = Co, M),[22] and Zr_6CoAs_2[23] contain extended 3D networks of the early transition element with late transition elements as interstitials, located in one-, two-, or three-capped trigonal prisms.

Trying to synthesize quaternary phosphides with two different early transition elements M and one late transition element M′ is assumed to substantially complicate the DFSO concept. In such a case, one has to consider three different trends, i.e. for the M−M, M−M′, and M−P interactions. Our first attempts yielded the novel $Hf_{4.96(4)}Nb_{5.04(4)}Ni_3P_5$, which forms a new

[†] Present address: Philipps-Universität Marburg, Fb Chemie, D-35032 Marburg, Germany.

[⊗] Abstract published in *Advance ACS Abstracts,* December 15, 1997.

(1) Yao, X.; Franzen, H. F. *J. Am. Chem. Soc.* **1991**, *113*, 1426−1427.
(2) Yao, X.; Miller, G. J.; Franzen, H. F. *J. Alloys Compd.* **1992**, *183*, 7−17.
(3) Yao, X.; Franzen, H. F. *J. Solid State Chem.* **1990**, *86*, 88−93.
(4) Yao, X.; Franzen, H. F. *Z. Anorg. Allg. Chem.* **1991**, *598/599*, 353−362.
(5) Yao, X.; Marking, G. A.; Franzen, H. F. *Ber. Bunsenges. Phys. Chem.* **1992**, *96*, 1552−1557.
(6) Franzen, H. F.; Köckerling, M. *Prog. Solid State Chem.* **1995**, *23*, 265−289.
(7) Marking, G. A.; Franzen, H. F. *Chem. Mater.* **1993**, *5*, 678−680.
(8) Cheng, J.; Franzen, H. F. *J. Solid State Chem.* **1996**, *121*, 362−371.
(9) Marking, G. A.; Franzen, H. F. *J. Alloys Compd.* **1994**, *204*, L17−L20.
(10) Harbrecht, B. *Z. Kristallogr.* **1988**, *182*, 118−120.
(11) Harbrecht, B.; Franzen, H. F. *J. Less-Common Met.* **1985**, *113*, 349−360.
(12) Harbrecht, B. *J. Less-Common Met.* **1986**, *124*, 125−134.
(13) Harbrecht, B. *J. Less-Common Met.* **1988**, *141*, *59*−71.
(14) Conrad, M.; Harbrecht, B. *J. Alloys Compd.* **1993**, *197*, 57−64.
(15) Wang, C.; Hughbanks, T. *Inorg. Chem.* **1996**, *35*, 6987−6994.
(16) Abdon, R. L.; Hughbanks, T. *Chem. Mater.* **1994**, *6*, 424−428.
(17) Abdon, R. L.; Hughbanks, T. *J. Am. Chem. Soc.* **1995**, *117*, 10035.
(18) Kleinke, H.; Franzen, H. F. *Angew Chem., Int. Ed. Engl.* **1997**, *36*, 513−516.
(19) Kleinke, H.; Franzen, H. F. *J. Solid State Chem.* **1997**, *131*, 379−386.
(20) Kleinke, H.; Franzen, H. F. *J. Alloys Compd.* **1996**, *229*, 40−53.
(21) Kleinke, H.; Franzen, H. F. *Chem. Mater.* **1997**, *9*, 1030−1035.
(22) Kleinke, H.; Franzen, H. F. *Inorg. Chem.* **1996**, *35*, 5272−5277.
(23) Kleinke, H. *J. Alloys Compd.* **1997**, *252*, L29−L31.

S0002-7863(97)01868-4 CCC: $14.00

Table 1. Cell Dimensions of $Hf_xNb_{10-x}Ni_3P_5$ with Varying x Parameter

x	a/Å	c/Å	V/Å^3
4[a]	9.5556(3)	3.5009(2)	276.84(2)
5[b]	9.561(4)	3.5237(5)	279.0(2)
5[a]	9.5698(7)	3.5250(4)	279.57(5)
6[a]	9.5870(4)	3.5373(3)	281.56(3)

[a] Cell dimensions obtained by indexing the powder diagram of the bulk sample. [b] Cell dimensions obtained from single crystal data.

structure type with three different M sites. All three M sites have short contacts to Ni as well as P sites. To our knowledge this is the first example of a fractional Hf/Nb occupation on different atom sites. We report here the synthesis, phase range, crystal and electronic structure, and physical properties. Calculations of the different bond orders and overlap populations help in understanding the different fractional site occupancies in this case also, proving the possibility of a more general use of the DFSO concept.

Experimental Procedures

Syntheses. The monophosphides HfP and NbP were prepared in sealed silica tubes at a maximum temperature of 800 °C, starting from the elements in the stoichiometric ratio (Hf: ALFA AESAR, powder, −325 mesh, purity 99.6% (containing 2−3.5% Zr); Nb: ALFA AESAR, powder, −60 mesh, purity 99.8%; P: ALFA AESAR, powder, −100 mesh, red amorphous, 99%). To avoid a high vapor pressure of elemental phosphorus, the samples were annealed at 500 °C over a period of 1 week. Thereafter, all phosphorus has reacted to form Hf and Nb phosphides, respectively. The tubes were then heated to 800 °C, and kept at that temperature for 3 days to obtain homogeneous monophosphides. The powder diagrams of the products experimentally obtained contained only the reflections of HfP and NbP, respectively. For the synthesis of $Hf_5Nb_5Ni_3P_5$ a stoichiometric mixture of 5 mmol of HfP, 5 mmol of Nb, and 3 mmol of M (FISHER, purified powder) was thoroughly mixed and then cold-pressed to a pellet. This pellet was arc-melted twice on a water-cooled copper hearth under an Argon flow with inversion of the sample after the first melt. Single crystals were obtained after annealing in a tungsten crucible in an induction furnace at 1350 °C under dynamic vacuum (10^{-6} bar) for 5 h. The Guinier diffraction pattern showed only the reflections of $Hf_5Nb_5Ni_3P_5$.

All our attempts to substitute any of the- metals of $Hf_5Nb_5Ni_3P_5$ failed. We arc-melted and annealed different samples of the initial compositions $(M^1)_x(M^2)_{10-x}M'_3P_5$ with M^1 = Zr, Hf; M^2 = Nb, Ta; M' = Co, Ni; and x = 0, 2.5, 4, 5, 6, 7.5, 10. The new structure discussed here occurred only in the Hf−Nb−Ni−P system. The powder diagrams of the samples with the starting compositions "$Hf_4Nb_6Ni_3P_5$" and "$Hf_6Nb_4Ni_3P_5$" consisted mainly of the reflections of the $Hf_xNb_{10-x}Ni_3P_5$ phase; only a few other, weak unidentified reflections were observed. Indexing of the three Guinier patterns of the samples with the initial compositions "$Hf_4Nb_6Ni_3P_5$", $Hf_5Nb_5Ni_3P_5$, and "$Hf_6Nb_4Ni_3P_5$" yielded the different lattice constants shown in Table 1. As expected on the basis of the different Pauling single bond radii for Hf (1.442 Å) and Nb (1.342 Å),[24] the cell dimensions increase significantly with increasing Hf content. It is concluded that $Hf_5Nb_5Ni_3P_5$ is not a line compound, but that the phase range of $Hf_xNb_{10-x}Ni_3P_5$ is rather small with $4 < x < 6$.

Electron Dispersive Spectroscopy (EDS). To check for adventitious impurities, i.e. W from the crucible or Cu from the Cu hearth, $Hf_5Nb_5Ni_3P_5$ crystals were scanned with a JSM-840A scanning microscope (JEOL). No impurities were found, and in all cases, all four elements, Hf, Nb, Ni, and P, were present. According to the standardless EDS analysis, the composition of the crystals was determined to be homogeneous within the range of the standard deviations of about ±10% for each element, which can be explained by the different orientations of the scanned surfaces.

Structure Determination. A needle-like single crystal isolated from a sample with the starting composition $Hf_5Nb_5Ni_3P_5$ was selected for data collection and mounted on a glass fiber. The crystal quality was checked with a Laue photograph, using a Weissenberg camera. The data were collected on a Rigaku AFC6R diffractometer equipped with graphite monochromated Mo Kα radiation and a 12KW rotating anode. The orientation matrix for the data collection and the preliminary cell constants were obtained from a least-squares refinement using 17 carefully centered reflections in the range $17.4° < 2\theta < 47.5°$. The ideal hexagonal lattice constants were refined to a = 9.561(4) Å, c = 3.5237(5) Å, and V = 279.0(2) Å^3. The good agreement with the cell dimensions obtained from the bulk sample confirms that the crystal is representative of the whole sample. Four octants were measured with the $\omega-2\theta$ technique to a maximum 2θ value of 70° and later merged. The intensities of three standard reflections, measured after every 100 reflections, remained constant throughout data collection. The data were corrected for Lorentz and polarization effects.

Table 2. Crystallographic Data for $Hf_5Nb_5Ni_3P_5$

empirical formula	$Hf_{4.96(4)}Nb_{5.04(4)}Ni_3P_5$
mol wt	1687.95 g/mol
temp of data collection	295 K
cryst dimens	0.02 mm × 0.002 mm × 0.002 mm
space group	$P\bar{6}2m$ (No. 189)
unit cell dimens	a = 9.561(3) Å, c = 3.5237(5) Å V = 279.0(2) Å^3
no. of formula units	1
calcd density	10.047 g/cm^3
abs coeff	56.23 mm^{-1}
F(000)	724
scan mode, scan width	$\omega-\theta$, $(1.21 + 0.34 \tan\theta)°$
scan speed	4.0 deg/min (in ω, 3 rescans)
range of 2θ	4−70°
no. of measured reflcns	2616
no. of independent reflcns	511 (R_{int} = 0.071)
no. of obsd reflcns ($I > 3\sigma(I)$)	267
no. of parameters refined	25
$R(F^2)$, $R_w(F^2)$, goodness of fit (GOF)	0.045, 0.054, 1.02
extinction coeff	0.74061×10^{-6}
max, min peak in final diff map	6.42 e$^-$/Å^3, −4.24 e$^-$/Å^3
abs corr	Ψ scan
min, max transmission	0.45−0.99

No systematic extinctions were found, and the distribution of the normalized structure factors pointed to a noncentrosymmetric space group. Thus, the highest reasonable symmetry is that of the space group $P6mm$. However, it turned out that the structure model obtained in this space group could be refined to reasonable residual factors, but one position (6d) was refined best as having a 1:1 mixed occupancy of nickel and phosphorus. Since all atoms were located either on z = 0 or $z = {}^1/_2$, that structure model could also be refined in the space group $P6/mmm$. Reducing the symmetry to $P\bar{6}2m$ occurs with two independent 3g positions instead of the 6d site, and yielded a structure that refined with fully occupied Ni and P sites. It is concluded that $P\bar{6}2m$ is the correct space group.

The structure was solved by direct methods, using the SHELXS-86 program package.[25] Six peaks with reasonable distances to each other (>2.1 Å) were taken from the e-map. The three strongest peaks all had different heights, and were thus considered as 100% occupied mixed Hf/Nb sites. According to their heights and interatomic distances, the three other peaks were identified as one Ni and two P positions. Final refinements of this model, using the TEXSAN program package,[26] yielded uniform temperature factors for all six positions. The occupancy factor was determined to be 100% Hf of the first metal site (M1), 59.5(4)% Hf and 40.5(4)% Nb of M2, and 13.1(6)% Hf and 86.9(6)% Nb of M3. This results in the empirical formula $Hf_{4.96(4)}Nb_{5.04(4)}Ni_3P_5$, which is, within the standard deviations, equal to the starting composition. The crystallographic data for $Hf_5Nb_5Ni_3P_5$ are summarized in Table 2, and the atomic positions, equivalent temperature factors, occupancy factors, and the anisotropic temperature factors, are contained in the Supporting Information.

(24) Pauling, L. *The Nature the Chemical Bond*, 3rd ed.; Cornell University Press: Ithaca, NY, 1948.

(25) Sheldrick, G. M. *SHEIXS-86*, Universität Göttingen: Germany, 1986.

(26) TEXSAN: *Single Crystal Structure Analysis Software, Version 5.0*; Molecular Structure Corporation: The Woodlands, TX, 1989.

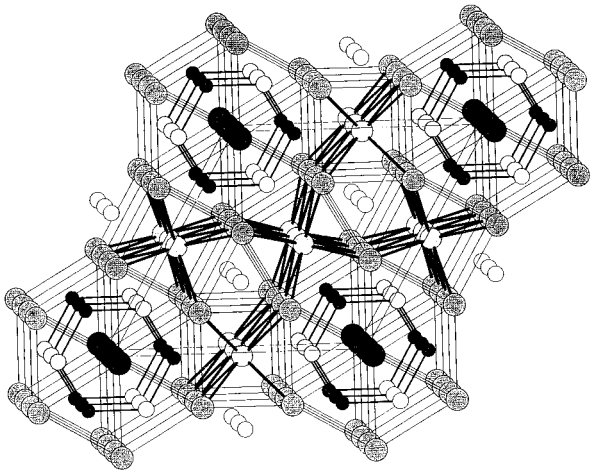

Figure 1. Projection of the structure of $Hf_5Nb_5Ni_3P_5$ along [001]: large, black circles, M1; large, heavily dotted circles, M2; large, medium dotted circles, M3; medium, white circles, P; small, black circles, Ni atoms. Only M−M and Ni−P bonds are shown; thicker lines, M−M bonds <3.1 Å.

Magnetic Susceptibilities. Magnetic data were obtained for the annealed bulk sample of $Hf_5Nb_5Ni_3P_5$. Temperature-dependent measurements were made at 3 T in the temperature range of 6−296 K on a Quantum Design MPMS SQUID magnetometer. The data were corrected for the diamagnetic atom cores.

Results and Discussion

$Hf_5Nb_5Ni_3P_5$ crystallizes in a new structure type, containing four crystallographically different metal sites and two different P positions. Of the four metal sites, one is a Ni position, one is occupied only by Hf (M1), and two have fractional Hf/Nb occupancies (M2 and M3). The crystal structure can be described on the basis of the early transition element substructure as follows. Cubes of M2 atoms, centered by M3, are condensed via opposite faces to form linear chains parallel to the *c* axis, and thus infinite *bcc* fragments. These chains are interconnected via common edges to a three-dimensional network, surrounding the P2 atoms in a trigonal prismatic arrangement. Six of these chains form a channel that is filled by the M1 atoms. The P1 and the Ni atoms are located in trigonal prisms formed by the M1 and M2 atoms. These prisms are interconnected sharing rectangular faces resulting in an AlB_2-like arrangement. Thus, the structure can formally be described as an intergrowth of the *bcc* and AlB_2 structure. Figure 1 shows the projection of the structure of $Hf_5Nb_5Ni_3P_5$ along [001], emphasizing the M−M and Ni−P bonds.

Each P atom is situated in a three-capped trigonal prism. The M_6P2 prism contains six M2 atoms at the corners and is capped by three M3 atoms. The corners of the M_6P1 prism are occupied with two M1 and four M2 atoms, and the caps are two Ni and one M3 atom. Similarly, the Ni atom is surrounded by two M1 and four M2 atoms, forming a trigonal prism that is three-capped by two P1 atoms and one M3 atom. Thus, the Ni and P1 coordination spheres are like those in Hf_5NiP_3[21] and Hf_2NiP.[18] The occurrence of both small atoms, Ni and P, as interstitial atoms in trigonal prismatic voids of the M substructure is very common in Hf rich hafnium nickel phosphides, but rather unusual for niobium nickel phosphides. The structure of $Nb_5Ni_4P_4$,[27] for example, contains chains of edge-condensed Ni_4 tetrahedra surrounded by octahedral vertex-condensed Nb_6P_8 chains. In this structure, P is located in a trigonal Nb_4Ni_2 prism, capped by one Ni and two Nb atoms. The only phosphide known today in the Nb/Ni/P system with a Nb/(Ni + P) ratio between 3/2 and 1/1 is Nb_3Ni_2P,[28] which structure has been reported as of the U_3Si_2 type with mixed Nb/Ni occupancies on one site and mixed Ni/P occupancies on the interstitial site, coordinated by Nb in a trigonal prism. This shows that it is possible to find Ni and P together on interstitial trigonal prismatic coordinated positions in Nb compounds; however, we have not been able to prepare any new niobium nickel phosphides with structures similar to those of M_2NiP (M = Zr, Hf), $Zr_9Ni_2P_4$, or Hf_5NiP_3.

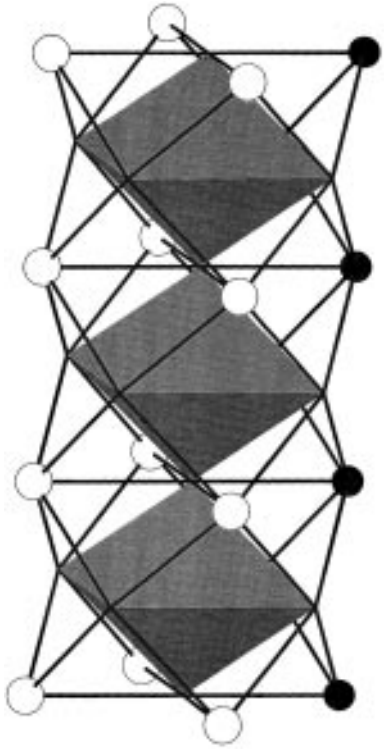

Figure 2. Chain of the vertex-condensed M_6 octahedra of $Hf_5Nb_5Ni_3P_5$: dotted areas, triangular faces of the octahedra; white circles, P; small, black circles, Ni atoms.

The second structure motif here, the chains of face-condensed centered cubes, is often observed in metal-rich phosphides, i.e. in the binaries Nb_7P_4[29] and Hf_7P_4,[30] and in the ternary $Zr_9M'P_4$.[22] In these three examples as well as in $Hf_5Nb_5Ni_3P_5$ the shortest M−M bonds of these units occur between the centers and the corners of the cubes. In the structure of $Hf_5Nb_5Ni_3P_5$, these short bonds have lengths of 3.005(3) and 3.047(4) Å, compared to the M−M distances along the edges of the cube between 3.5237(5) A along [001] and 3.40 and 3.56 Å in the *ab* plane. A comparison to Nb_7P_4 and Hf_7P_4 shows that the short M−M distances found in $Hf_5Nb_5Ni_3P_5$ are just between the corresponding averaged distances in Nb_7P_4 (2.98 Å) and Hf_7P_4 (3.11 Å), where M centered M cubes also occur, as expected, based on the fractional Hf/Nb site occupancies in case of $Hf_5Nb_5Ni_3P_5$.

From another point of view, these chains of centered cubes may be regarded as chains of vertex-condensed (empty) octahedra, as discussed for a series of compounds, including Nb_7P_4, by Simon.[31] The Ni and P atoms would then cap the triangular faces of the octahedra (Figure 2), and the resulting

(27) Berger, R.; Phavanantha, P.; Mogkolsuk, M. *Acta Chem. Scand.* **1980**, *34A*, 77.

(28) Lomnitskaya, Y. F.; Kuz'ma, Y. B. *Inorg. Mater.* **1983**, *19*, 1191−1195.

(29) Rundqvist, S. *Acta Chem. Scand.* **1966**, *20*, 2427−2434.

(30) Kleinke, H.; Franzen, H. F. *Angew. Chem., Int. Ed. Engl.* **1996**, *35*, 1934−1936.

(31) Simon, A. *Angew. Chem., Int. Ed. Engl.* **1981**, *20*, 1−22.

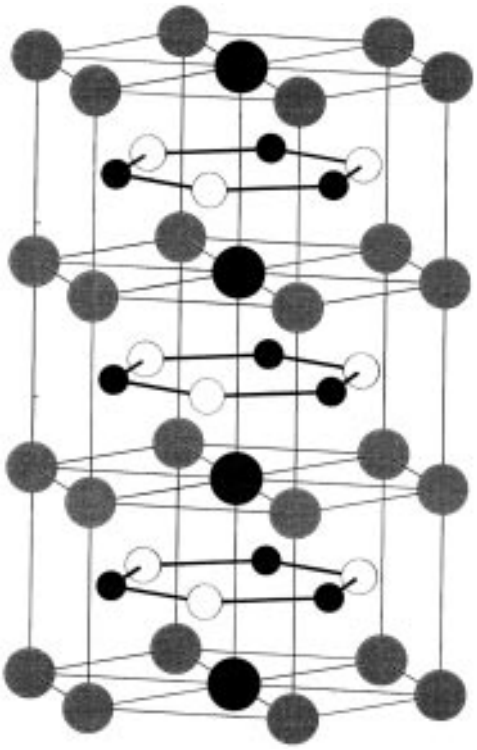

Figure 3. Coordination sphere of the M1 atom of $Hf_5Nb_5Ni_3P_5$: large, black circles, M1; large, dotted circles, M2; medium, white circles, P; small, black circles, Ni atoms.

structure motif is that of the M_6X_8 clusters as observed in the Chevrel phases, having the metal atom Ni and the nonmetal atom P as X. A comparable observation was made in the structure of $Zr_9Ni_2P_4$,[22] where Ni and P cap the triangular faces of the double octahedra Zr chain. The distances and angles within these units in case of $Hf_5Nb_5Ni_3P_5$, however, are very close to those of an ideal cube, i.e. of a strongly shortened octahedron. The advantages of describing these chains as condensed M_6X_8 clusters are (i) that this description already includes the relative locations of the X positions and (ii) that this links the solid state structures to the common M_6 octahedra in the solution chemistry, making this concept mnemonically very useful.

In contrast to the M2 and M3 atoms, the M1 atom does not form any M−M distances shorter than 3.5 Å, which is rather unusual for a M-rich phosphide. The shortest M1−M distances are along the *c* axis (3.5237(5) Å), six other comparable M1−M distances are in the *ab* plane (d_{M1-M2} = 3.560(2) Å). This coordination sphere (Figure 3) is completed by six Ni and six P1 atoms at shorter distances (ca. 2.8 Å), which form interpenetrating trigonal $MlNi_6$ and $M1P_6$ prisms. A similar Zr coordination is found for the Zr site in the structure of ZrNiP.[32] In the structure of ZrNiP, the Ni and P sites alternate along *c*, and thus Zr is located in interpenetrating ZrP_6 and $ZrNi_6$ octahedra.

To investigate the reasons for the occurrence of different fractional Hf/Nb occupancies of the M sites, we calculated the Pauling bond orders (using Pauling's equation $d(n) = d(1) - 0.6 \log n$, with n = bond order, r_{Hf} = 1.442 Å, r_{Nb} = 1.342 Å, r_{Ni} = 1.154 Å, and r_p = 1.100 Å)[24] for all three M sites. Furthermore, we calculated the electronic structure using the extended Hückel approximation.[33,34] The parameters for Hf and Nb were taken from solid state charge iterations, performed on Hf_7P_4 and Nb_7P_4,[35] the P parameters from Clementi and Roetti.[36] The Ni parameters were obtained from charge iteration on $Zr_9Ni_2P_4$, where Ni is situated in a trigonal Zr_6 prism, capped by one Zr and two P atoms. A list of the Hückel parameters is given in Table 3.

Table 3. Parameters for EH Calculations

orbital	H_{ii}/eV	ζ_1	c_1	ζ_2	c_2
Hf, 6s	−8.58	2.21			
Hf, 6p	−4.98	2.17			
Hf, 5d	−8.71	4.36	0.6967	1.709	0.5322
Nb, 5s	−8.62	1.89			
Nb, 5p	−4.79	1.85			
Nb, 4d	−9.28	5.75	0.6401	1.640	0.5516
Ni, 4s	−8.62	1.93			
Ni, 4p	−4.28	1.93			
Ni, 3d	−11.06	5.75	0.5862	2.200	0.5845
P, 3s	−18.60	1.88			
P, 3p	−12.50	1.63			

Table 4. Selected Interatomic Interactions for $Hf_5Nb_5Ni_3P_5$

		distance/Å	no.	PBO[a]	PBO[b]	MOP[a]	MOP[b]
M1	M1	3.5237(5)	2×	0.09	0.04	0.076	0.052
M1	M2	3.560(2)	6×	0.07	0.03	0.092	0.060
M1	Ni1	2.800(3)	6×	0.46	0.31	0.086	0.081
M1	P1	2.806(8)	6×	0.37	0.25	0.264	0.239
M2	M1	3.560(2)		0.07	0.03	0.092	0.060
M2	M2	3.395(2)	2×	0.14	0.07	0.099	0.079
M2	M2	3.5237(5)	2×	0.09	0.04	0.057	0.038
M2	M2	3.560(2)		0.07	0.03	0.131	0.092
M2	M2	3.561(2)		0.07	0.03	0.044	0.036
M2	M3	3.005(3)	2×	0.63	0.29	0.318	0.261
M2	M3	3.047(4)	2×	0.54	0.25	0.235	0.197
M2	Ni1	2.664(2)	2×	0.77	0.53	0.168	0.157
M2	P1	2.661(3)	2×	0.63	0.43	0.315	0.297
M2	P2	2.6353(8)	2×	0.70	0.48	0.330	0.318
M3	M2	3.005(3)	4×	0.63	0.29	0.318	0.261
M3	M2	3.047(4)	4×	0.54	0.25	0.235	0.197
M3	M3	3.5237(5)	2×	0.09	0.04	0.149	0.104
M3	Ni1	2.567(7)		1.12	0.76	0.227	0.212
M3	P1	2.63(1)		0.69	0.47	0.314	0.300
M3	P2	2.760(1)	2×	0.43	0.29	0.244	0.237
Ni	P1	2.180(4)	2×	1.33	1.33	0.304	0.337

[a] As obtained for model **I**: "$Hf_{10}Ni_3P_5$" with a *vec* = 100 e^-. [b] As obtained for model **II**: "$Nb_{10}Ni_3P_5$" with a *vec* = 100 e^-.

Since the Hückel model does not directly provide a possibility of calculations of structures with mixed occupied atom sites, we calculated the electronic structures and bond orders for two models, each of which has only one kind of M atom, i.e. model **I** ("$Hf_{10}Ni_3P_5$") and model **II** ("$Nb_{10}Ni_3P_5$"). In both cases, we calculated the Fermi levels for a valence electron concentration per formula unit of *vec* = 100 e^-, which corresponds to the formula $Hf_5Nb_5Ni_3P_5$. Treating the three metal positions equally leads to a comparison of sites which is independent of the occupancy factors. Thus, this comparison should give an insight why Nb prefers the M3 site and Hf the M1 site. Interatomic distances and their PBOs and MOPs are listed in Table 4, the sums of the PBOs and MOPs in Table 5.

A comparison of the densities of states for models **I** (Figure 4) and **II** (Figure 5) reveals the similarity of these two models. The energetically higher ionization potential of the d states of Hf, compared to Nb d states (−8.71 eV vs. −9.28 eV), leads to a higher Fermi level in the case of model **I** (E_F(**I**) = −8.95 eV,

(32) Kleinke, H.; Franzen, H. F. *Z. Anorg. Allg. Chem.* **1996**, *622*, 1893−1900.
(33) Hoffmann, R. *J. Chem. Pays.* **1963**, *39*, 1397−1412.
(34) Whangbo, M.-H.; Hoffmann, R. *J. Am. Chem. Soc.* **1978**, *100*, 6093−6098.
(35) Kleinke, H. Unpublished research.
(36) Clementi, E.; Roetti, C. *At. Nucl. Data Tables* **1974**, *14*, 177−478.

Table 5. Sums of Pauling Bond Orders and Mulliken Overlap Populations for $Hf_5Nb_5Ni_3P_5$

		PBO[a]	PBO[b]	MOP[a]	MOP[b]
M1	M	0.60	0.26	0.704	0.464
M1	Ni	2.76	1.86	0.516	0.486
M1	P	2.22	1.50	1.584	1.434
M2	M	3.01	1.39	1.685	1.338
M2	M	1.54	1.06	0.336	0.314
M2	P	2.66	1.82	1.296	1.230
M3	M	4.86	2.24	2.510	2.040
M3	Ni	1.12	0.76	0.227	0.212
M3	P	1.55	1.05	0.802	0.774

[a] As obtained for model **I**: "$Hf_{10}Ni_3P_5$" with a *vec* = 100 e^-. [b] As obtained for model **II**: "$Nb_{10}Ni_3P_5$" with a *vec* = 100 e^-.

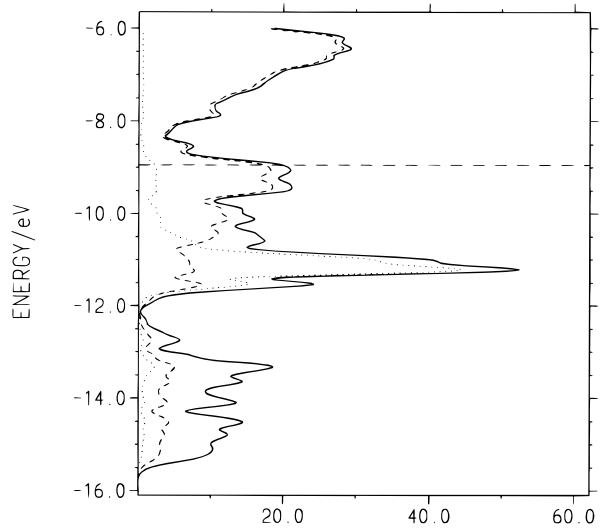

Figure 4. Densities of states (DOS) for model **I**: dashed horizontal line, Fermi level (−8.95 eV); solid curve, total DOS; dashed curve, Hf; dotted curve, Ni contributions.

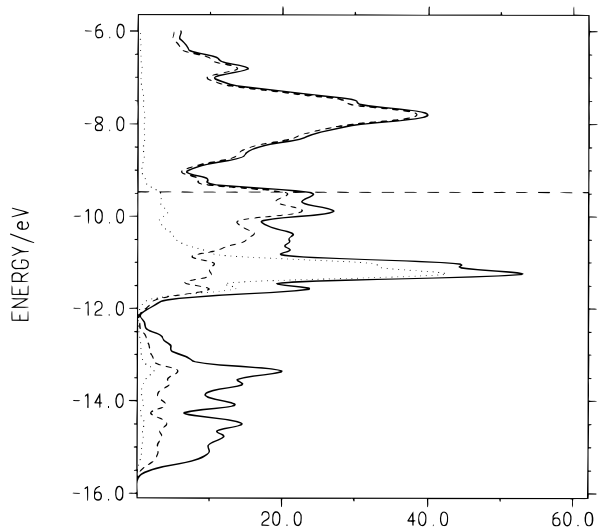

Figure 5. Densities of states (DOS) for model **II**: dashed horizontal line, Fermi level (−9.47 eV); solid curve, total DOS; dashed curve, Nb; dotted curve, Ni contributions.

E_F(**II**) = −9.47 eV) and to a lower M contribution at the Fermi level, because Hf is more oxidized than Nb. Qualitatively, both figures resemble each other. At low energies, below −12 eV, the p orbitals of P occur with some contribution of the metal atoms, showing covalent mixing with the M and Ni states. The 3d states of Ni form a sharp peak slightly below −11 eV, which overlaps with the Hf or Nb states. M contributions at the energy

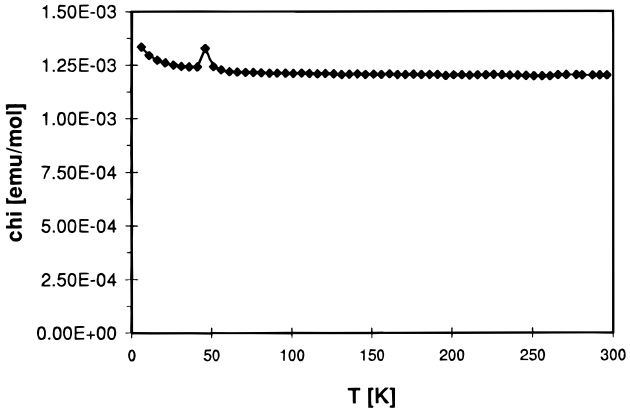

Figure 6. Temperature dependence of the magnetic susceptibilities for $Hf_5Nb_5Ni_3P_5$.

of the Ni states show the covalency of the M−Ni interactions. Basically, only M states are found at the Fermi level for both models.

The significant density of states at the Fermi level suggests metallic behavior, considering the numerous M−M interactions in all three dimensions. The expectation of metallic properties is confirmed by the experimentally observed, almost temperature independent weak Pauli paramagnetism, obtained from the polycrystalline bulk sample of $Hf_5Nb_5Ni_3P_5$ as shown in Figure 6. On the basis of the three-dimensional M network, anisotropic properties are not expected. The magnetic susceptibility at room temperature of 1.2×10^{-3} emu/mol is somewhat higher than the doubled magnetic signal of Hf_5NiP_3 (4.7×10^{-4} emu/mol),[21] and the formula contains twice as many atoms per mole. In both cases, the M/(Ni + P) ratio is exactly 5/4, which means that the M atoms are oxidized by Ni and P to a comparable extent, occurring with a higher density of states at the Fermi level in the case of the Nb compound because of the higher valence electron number per M atom. Thus, a relatively slightly higher magnetic susceptibility is expected, because the susceptibility is (in the case of Pauli paramagnetism) proportional to the number of states at the Fermi level. The similarity of the structures of Hf_5NiP_3 and $Hf_5Nb_5Ni_3P_5$, with respect to the Ni and P coordination spheres, renders such a comparison possible.

The higher electronegativity as well as the higher number of valence electrons of Nb, compared to Hf, should lead to a higher Nb/Hf ratio on the less oxidized M sites. The atomic contributions of one M1 (solid curve), one M2 (dotted curve), and one M3 atom (dashed line), as calculated for model **I**, are compared in Figure 7. It is evident that the M3 states are significantly more filled than the M2 states, and the M1 atom is the most oxidized one. This is in good coincidence with the increasing Nb content from M1 (0%) over M2 (40.5(4)% Nb) to M3 (86.9%).

A comparison of all of the different M−M, M−Ni, and M−P interactions is necessary for an understanding of the fractional site occupancies, because the M−X (X = Ni or P) interactions cannot be neglected with a small M/X ratio of 1.25. This is in contrast to the use of the DFSO concept in the quasibinary Nb/Ta sulfides with a M/S ratio ≥2, in which case calculations of the M−M bond orders were sufficient.

Hf as the more electropositive atom is most likely the better bonding partner to the most electronegative atom in the compound, which is P in this case. The same is true for the M−Ni bonds: according to Brewer and Wengert,[37] the Lewis acid/Lewis base interaction is stronger between Hf and Ni than between Nb and Ni for two reasons. First, the higher electron

(37) Brewer, L.; Wengert, P. *R. Metall. Trans.* **1973**, *4*, 83−104.

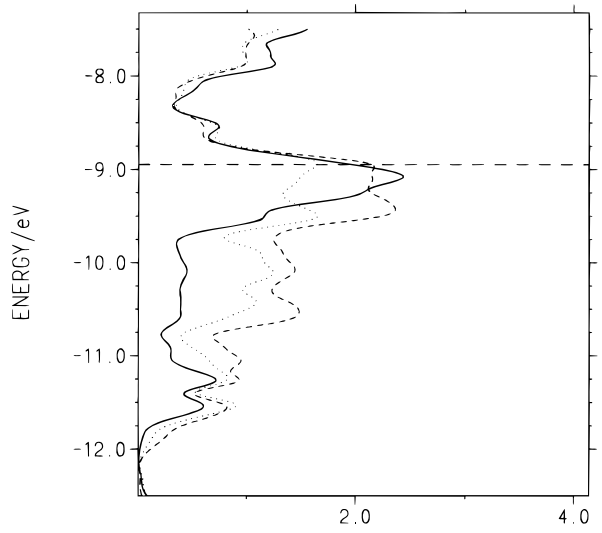

Figure 7. Weighted partial contributions of the different M atoms (model **I**): dashed horizontal line, Fermi level (−8.95 eV); solid curve, M1; dotted curve, M2; dashed curve, M3 contributions per M atom.

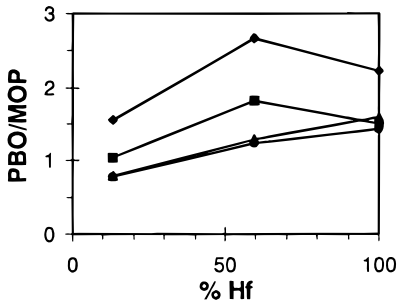

Figure 8. Sum of the Pauling bond orders and Mulliken overlap populations of the M−P interactions: diamonds, PBO(Hf−P), model **I**; squares, PBO(Nb−P), model **II**; triangles, MOP(Hf−P), model **I**; circles, MOP(Nb−P), model **II**.

deficiency of Hf makes Hf the better acid, and second, the 5d−3d interactions are stronger than the 4d−3d interactions. The latter statement is also valid for the (pseudo)homonuclear M−M bonds, but the higher number of electrons available for Nb, as discussed above, enables Nb to form more metal−metal bonds.

First, we discuss the metal−phosphorus bonds. The Pauling bond orders for all the metal−phosphorus interactions vary from 0.37 for M1−P1 in model **I** to 1.33 for the Ni−P1 bond. Thus, bonding character can be assumed in all these cases. In addition, the short length of the Ni−P1 bond of 2.180(4) Å, which is shorter than the sum of the Pauling single bond radii, prohibits a substitution of Ni by the bigger Co ($r_{Co} = 1.162$ Å). Slightly shorter Ni−P distances are found for (not fully occupied) Ni sites in two related structures, $Hf_5Ni_{1+x}P_3$[21] and $HfNi_xP$,[38] where also no analogous Co phosphides are known.

It is not surprising to find positive overlap populations for the M−P bonds. As shown in Figure 8, the sums of the overlap populations increase with increasing Hf content per M position. The maximum for the Pauling bond orders at 59.5% Hf (M2) shows the limits of the Pauling model, which is only based on distances. As a consequence, this model always yields wrong bond orders when any matrix effects occur. Considering the overlap populations calculated with the extended Hückel approximation as the more precise values, the PBO for the M2−P bond is too high, as a comparison with the corresponding values for the M1−P and M3−P bonds shows. It can be concluded

(38) Kleinke, H.; Franzen, H. F. *Z. Anorg. Allg. Chem.* **1996**, *622*, 1342−1348.

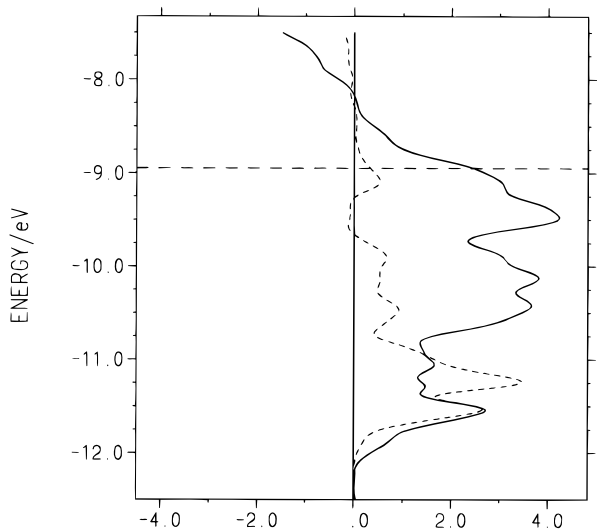

Figure 9. Selected crystal orbital overlap populations for model **I**: dashed, horizontal line, Fermi level; solid curve, M−M; dashed curve, M−Ni interactions; left side, antibonding interactions (−); right side, bonding (+).

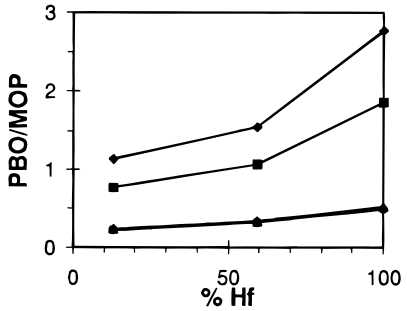

Figure 10. Sum of the Pauling bond orders and Mulliken overlap populations of the M−Ni interactions: diamonds, PBO(Hf−Ni), model **I**; squares, PBO(Nb−Ni), model **II**; triangles, MOP(Hf−Ni), model **I**; circles, MOP(Nb−Ni), model **II**.

that the M2−P distances are shorter than expected on the basis of their actual bond orders, probably because of some matrix effects. As will be discussed later in this article, the correlation between MOP and PBO is better for the M−M and M−Ni interactions. Thus, these two models support each other. Giving greater weight to the MOP it is concluded that the larger fractional occupancy of sites with higher M−P bond order is favored by the greater electronegativity difference between Hf and P in comparison with Nb and P.

Second, the M−Ni distances, ranging from 2.567(7) to 2.800(3) Å, have similar Pauling bond orders. The bonding character of these polar intermetallic interactions can be understood on the basis of the Lewis' acid/base concept, considering Hf/Nb as the acid and Ni as the base. Bonding Hf−Ni interactions also occur in the related ternary phosphides $Hf_5Ni_{1+x}P_3$, Hf_2NiP, HfNiP, and $HfNi_xP$, which all have Ni in the trigonal prismatic Hf coordination. As for models **I** and **II**, no antibonding M−Ni states are filled, which is shown for the Hf−Ni interactions in Figure 9 (dashed curve), calculated with model **I**. At the Fermi level, only a small number of the bonding Hf−Ni interactions occur, which is also true for the M−P interactions. This shows that the different *vec*'s for Hf and Nb play only a minor role for the differences in M−Ni and M−P interactions between the Hf and Nb-rich sites.

A graphic comparison of the M−Ni bond orders and overlap populations of the different M sites is made in Figure 10. As for the M−P interactions, the overall strength of the M−Ni

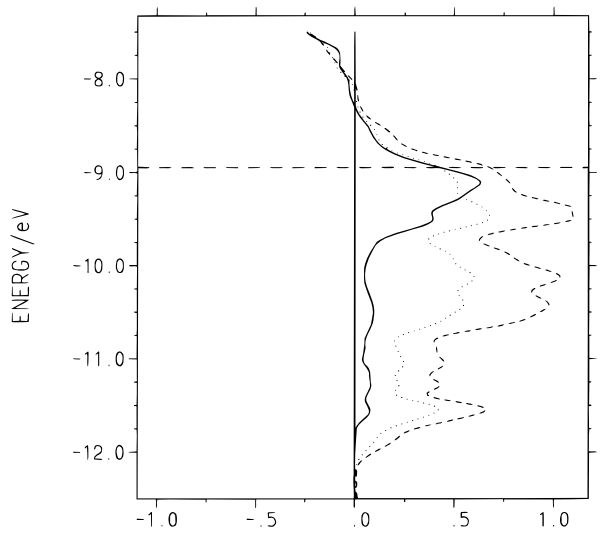

Figure 11. Selected crystal orbital overlap populations for model **I**: dashed, horizontal line, Fermi level; solid curve, M1−M; dotted curve, M2−M; dashed curve, M3−M interactions; left side, antibonding interactions (−); right side, bonding (+).

interactions increases with increasing Hf content. This can be considered as an indirect proof of the ideas of Brewer and Wengert, showing that Hf, compared to Nb, does form stronger M−Ni bonds.

The third kind of important interactions in the structure of $Hf_5Nb_5Ni_3P_5$ are the (pseudo)homonuclear interactions between the early transition elements. As shown in Figure 9 (solid curve), the M−M interactions play an important role in stabilizing this structure. Also, these are the only interactions with a significant contribution at the Fermi level. As a consequence, any changes in the valence electron concentration would change the M−M bonding. However, the metal−metal bonding is clearly not optimized for *vec* = 100 e^-; an additional six electrons would increase M−M and M−Ni bonding by raising the Fermi level to −8.2 eV.

The large number of filled M−M bonding states at the Fermi level implies that the increase by one in the number of valence electrons between Hf and Nb determines the preference of Nb for the positions with higher M−M bond order. The crystal orbital overlap populations for the different M−M interactions are clearly highest for M3 (dashed curve in Figure 11, using model **I**) and lowest for M1 (solid curve in Figure 11). A comparison of the Pauling bond orders and overlap populations for models **I** and **II** shows the clear preference of Nb for the sites with the highest M−M bond order (Figure 12). It is concluded that the different electron count is more important here than the different size of the d orbitals of Hf and Nb.

The results of the calculations of the overlap populations confirm that the shortest M−M bonds, i.e. those between the center and the corners of the cubes, are the strongest with MOPs of 0.318 and 0.235 for model **I**. On the other hand, the M2−M2 bond along the shortest edge of the M_8 cube (3.395(2) Å) has a MOP of only 0.099, compared to a MOP = 0.131 of the longer bond (3.560(2) Å) perpendicular to the M3−Ni bond. It is concluded that the electron deficiency of P leads to a local decrease of the M2 centered electrons available for the M2−M2 bonds in proximity to P. Similarly, a very small overlap population of 0.044 is calculated along the fourth edge of the cube which is perpendicular to a M3−P bond. In accordance with this, the MOP of the M3−M3 bond along the *c* axis (3.5237(5) Å) is rather high (0.149 in model **I**), because the P

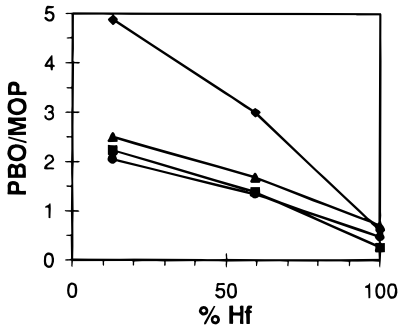

Figure 12. Sum of the Pauling bond orders and Mulliken overlap populations of the M−M interactions: diamonds, PBO(Hf−Hf), model **I**; squares, PBO(Nb−Nb), model **II**; triangles, MOP(Hf−Hf), model **I**; circles, MOP(Nb−Nb), model **II**.

atoms are not as close to the M3−M3 bond, and the parallel M2−M2 bond, being literally surrounded by P atoms, has a much smaller MOP of 0.057.

It is not surprising that we have been unable to prepare isostructural phosphides by substituting for any of the metal atoms, given the fact that all the metal-rich ternary phosphides and chalcogenides mentioned in the introduction, with the exception of $M_2M'P$ (M = Zr, Hf; M′ = Co, Ni), are unique for each early transition element. In particular, a replacement of Nb by Ta is unlikely because of the preference of Ta for structures other than those containing *bcc* units, which a comparison of the binary sulfides shows. The Nb sulfides $Nb_{21}S_8$[39] and $Nb_{14}S_5$[40] form structures containing in part *bcc* arrangements of the metal atoms, whereas the structures of the Ta sulfides Ta_2S[41] and Ta_6S (in both modifications[42,43]) consist of chains of Ta centered pentagonal antiprisms of Ta atoms. On the other hand, Zr tends to form *bcc* units (compare for example Zr_2S[44] with Hf_2S,[45] or $Zr_9Ni_2P_4$ with Hf_5NiP_3), suggesting that Zr does not readily replace Hf in $Hf_5Nb_5Ni_3P_5$, because in this compound the majority (92%) of the Hf atoms are not in cubic coordination. In addition, the structure does not form in either of the ternary systems, Hf−Ni−P or Nb−Ni−P, probably because an occurrence of one kind of metal atom on three such different atom sites in one structure is most unlikely, i.e. mixed occupancy favors structural complexity through diversity of metal-atom sites.

Acknowledgment. H.K. thanks the Deutsche Forschungsgemeinschaft for financial support of this work. The Ames Laboratory is operated for the US Department of Energy by Iowa State University under Contract No. W-7405-Eng-82. This research was also supported by the Office of the Basic Energy Sciences, Materials Science Division, Department of Energy.

Supporting Information Available: Tables of atomic positions, equivalent temperature factors, occupancy factors, and anisotropic thermal parameters for $Hf_5Nb_5Ni_3P_5$ (4 pages). See any current masthead page for ordering and Internet access instructions.

JA9718681

(39) Franzen, H. F.; Beinecke, T. A.; Conard, B. R. *Acta Crystallogr.* **1968**, *B24*, 412−416.
(40) Chen, H. Y.; Tuenge, R. T.; Franzen, H. F. *Inorg. Chem.* **1973**, *12*, 552−555.
(41) Franzen, H. F.; Smeggil, J. G. *Acta Crystallogr.* **1969**, *B25*, 1736−1741.
(42) Franzen, H. F.; Smeggil, J. G. *Acta Crystallogr.* **1970**, *B26*, 125−129.
(43) Harbrecht, B. *J. Less-Common. Met.* **1988**, *138*, 225−234.
(44) Conard, B. R.; Franzen, H. F. *High Temp. Sci.* **1971**, *3*, 49−55.
(45) Franzen, H. F.; Graham, J. *Z. Kristallogr.* **1966**, *123*, 133−138.